

## A modeling study of pre-processing considerations for reverse-time migration

Ian F. Jones<sup>1</sup>

### ABSTRACT

Much of the thinking behind conventional geophysical processing assumes that we wanted to image energy that propagates down from the surface of the earth, scatters from a reflector or diffractor, and then propagates back up to the recording surface without being reflected by any other feature. Such travel paths conform to the assumptions of one-way wave propagation, and most contemporary migration schemes are designed to image such data. In addition, the moveout behavior of these primary reflection events in the various prestack domains is well understood, and many of our standard data-preprocessing techniques relied on the assumption that this behavior adequately describes the events we wanted to preserve for imaging. As a corollary, events that do not conform to this prescribed behavior are classified as noise, and many of our standard preprocessing techniques

were designed to remove them. We assessed the kinematics of moveout behavior of events that arise from two-way wave propagation and the effect of certain preprocessing techniques on those events. This was of interest to us because the recent rapid increase in available cost-effective computing power has enabled industrial implementation of migration algorithms—particularly reverse-time migration—that in principle can image events that reflect more than once on their way from source to receiver. We used 2D synthetic data to show that some conventional data-processing steps—particularly those used in suppression of complex reverberations (“multiples”)—remove nonreverberatory primary events from seismic reflection data. Specifically, they remove events that have repeated or turning reflections in the subsurface (such as double-bounce arrivals) but that otherwise are imageable using reverse-time migration.

### INTRODUCTION

Recent enhancements to the speed and cost-effectiveness of computers now permit us to implement solutions of the wave equation that are more complete than those commonly used in the past (Baysal et al., 1983; Whitmore, 1983; McMechan, 1983; Bednar et al., 2003; Yoon et al., 2003; Shan and Biondi, 2004; Zhou et al., 2006; Zhang et al., 2006). The restriction to one-way propagation can be lifted, and data can be migrated to take advantage of more esoteric propagation paths, such as turned rays, double-bounce arrivals, and, potentially, multiples (Mittet, 2006). However, to take advantage of these improved algorithms, we must ensure that the data that are input to migration have not been compromised significantly. Specifically, we address the moveout behavior of double-bounce events (Hale et al., 1992; Hawkins et al., 1995; Bernitsas et al., 1997; Cavalcata and Lailly, 2005; Jones, 2008) and we note how some conventional preprocessing algorithms can damage those arrivals, thus ren-

dering superfluous certain aspects of any subsequent high-end migration.

We commence our analysis by using forward modeling to create synthetic data that show the moveout behavior of certain simple double-bounce events (referred to as “prism waves” by some authors) and turning-wave arrivals. To facilitate our demonstration, we first employ a ray-trace package with which we can model individual selected arrivals, and later we create more-complex synthetic data using a finite-difference (FD) technique. Brief details of these packages are given.

After we investigate the moveout behavior of the simple models, we move on to a model representing a complex North Sea salt-dome structure (Davison et al., 2000; Thomson, 2004; Farmer et al., 2006; Jones et al., 2006). Using synthetic data, we show the effect of various conventional preprocessing steps on double-bounce arrivals, and then we carry these analyses through to migration with a 2D reverse-time migration (RTM) algorithm capable of imaging the double-bounce arrivals. Jones (2008) gives a review of this modeling

Manuscript received by the Editor 27 November 2007; revised manuscript received 11 February 2008; published online 24 October 2008.

<sup>1</sup>ION GX Technology EAME, Egham, Surrey, U. K. E-mail: ian.jones@iongeo.com.

© 2008 Society of Exploration Geophysicists. All rights reserved.

work and its effect on real data. In the present paper, we expand on the synthetic modeling work that underpinned the North Sea study.

## MODELING AND MIGRATING 2D SYNTHETIC DATA

Although in principle many physical phenomena are conceptually simple, the resulting manifestations of the phenomena can be complex and difficult to understand in detail. Given this assertion, we note that great insight can be obtained through modeling studies. Such studies help us to understand, in a piecemeal sense, how simple elements of the process contribute to the complex whole.

We commence our studies using ray-trace modeling, wherein we can specify the creation of raypaths one at a time and in so doing we can isolate each contributing raypath from an otherwise confusing whole. Once we have identified the behavior and appearance of each contributing raypath, we progress to full elastic modeling to produce complete seismograms that are suitable to be used as input to preprocessing routines. In this work, we proceeded as follows.

First, we generated isotropic acoustic ray-traced 2D common-midpoint (CMP) data as a control to identify various individual arrivals. Initial data creation and analyses were performed for simple geometries and then repeated for a complex North Sea salt-diapir model. The data were created with 2-ms sampling, a peak frequency of approximately 35 Hz, a shot interval of 50 m, a CMP interval of 6.25 m, and a 6-km maximum offset.

Next, we generated more-realistic, elastic 2D FD shot-gather data for the complex North Sea salt-diapir model. Those modeled data used the same vertical interval-velocity model that the ray-trace model used, and they were created with 1-ms sampling (resampled to 4 ms for processing) and a peak frequency of approximately 17 Hz. In this study, we used an absorbing-surface boundary; hence, the FD data have no free-surface multiples. Because the modeling was conducted in 2D, we had no complex multiples resulting from out-of-plane scatterers that otherwise would resemble the double-bounce reflectors being considered here. Thus, we chose to simplify our procedures by avoiding creation of the more obvious multiples in the input data. Also, for the analyses being conducted here, we considered that acoustically modeled data would have been sufficient. However, these data also were being used in another study to assess the importance of converted-mode arrivals for this salt geometry, so we produced elastic FD data.

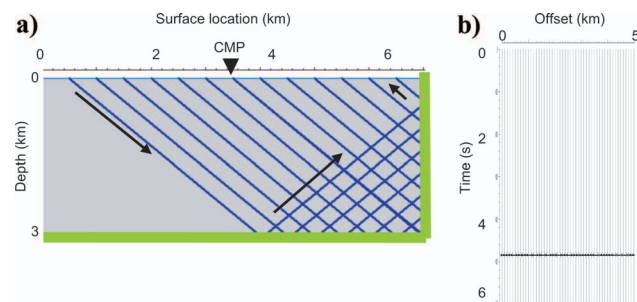


Figure 1. (a) Model horizons, in green, with sample raypaths, arrows indicating propagation direction, sample CMP location. (b) The resulting CMP gather with the arrival events shown. Right-angle corner reflector traveltimes are constant with offset: i.e., no moveout.

The explicit 2D/3D elastic FD wave-propagation code used for modeling seismic waves is fourth-order accurate in space and second-order accurate in time and is based on the elastodynamic formulation of the wave equation on a staggered grid (Madariaga, 1976; Virieux, 1986; Levander, 1988; Larsen and Gieger, 1998).

Next, we applied various processing techniques to the FD data using conventional data-processing flows that are likely to damage double-bounce events, including (1) a  $\tau$ - $p$  mute for backscattered noise, (2) a Radon demultiple, and (3) a CMP-domain apex-shifted demultiple (Trad, 2003; Stewart, 2004).

Finally, we performed 2D RTM after each preprocessing flow (all gathers input to RTM had a mute on the direct arrival) and we assessed the preservation of double-bounce arrivals in the resultant images.

### Simple models

We commenced by looking at three simple constant-velocity scenarios and one vertical-compaction-gradient scenario. These were a simple right-angle corner reflector, an acute-angle reflector with noncrossing rays, an acute-angle reflector with crossing rays, and an acute-angle reflector with a vertical compaction gradient to produce turning rays. For obtuse-angle geometry, we did not have double-bounce arrivals for this acquisition layout—we would need extremely long offsets and large arrival times to see such arrivals.

In Figures 1–4, we display the four modeled scenarios. In each figure we show the model and raypaths in part (a) and an associated CMP gather in part (b). It is clear that the moveout behavior does not conform to what we expect for normal one-way arrival paths but instead more closely resembles events such as those resulting from scattered energy or diffracted multiples. We know that for simple quasi-1D cylindrical models, all coaxially recorded events in a CMP gather will appear with their apexes at zero offset. This observation guides the design principle of various multiple-suppression techniques and the justification for muting in  $\tau$ - $p$  space to suppress backscattered energy. The corner reflector in Figure 1 shows no arrival-time moveout with offset. The noncrossing rays in Figure 2 show linearly decreasing arrival time with offset, and the crossing rays of Figure 3 show linearly increasing arrival time with offset. Here the terms *crossing* and *noncrossing* refer to the behavior of the initial downgoing and final upcoming raypath segments. The turning-ray arrivals (Hale et al., 1992) shown in Figure 4 resemble the noncrossing family of double-bounce events. For a right-angle corner reflector, the turning arrivals behave as in Figure 1, in that they also would show no moveout with offset. To obtain turning arrivals, we need a

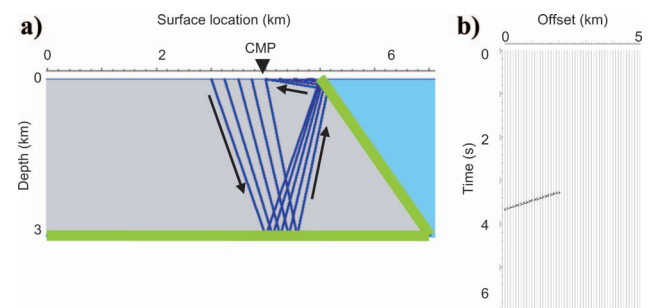


Figure 2. (a) Acute-angle, noncrossing events. Model horizons in green. (b) The associated CMP gather. Arrivals are present only on the near offsets, with arrival time decreasing with offset.

significant vertical velocity gradient in the model. In this case, with the midpoint only a few kilometers from the steep wall, we required a gradient of 3.0 ms/m. For midpoints farther from the steep event, gradients larger than approximately 0.2 ms/m will produce turning-ray arrivals.

**North Sea diapir model**

We now look at a full synthetic data set created along a 2D crestal line of a model representing a North Sea example, and we show the effects of various preprocessing techniques on these data. The velocity field used in the forward modeling was a simplified version of that derived during a prestack-depth-migration (PSDM) processing project of a real North Sea example. The velocity field is characterized by the density profile shown in Figure 5, and the interval-velocity profile is shown in Figure 6.

For steep salt bodies set in a background velocity field that exhibits a vertical compaction gradient, it is common to encounter turning-ray arrivals that are useful in imaging overturned salt walls. However, in this region of the North Sea, we have a velocity inversion in the overburden sediments at a depth of approximately 1 km; such inversions often preclude useful turning energy. Preliminary tests indicated that for our velocity structure, turning arrivals were unable to illuminate the overhanging salt walls; hence, we did not consider them in the detailed analysis we conducted in the rest of this paper. In other environments, turning arrivals also would be of interest and would behave similarly to the double-bounce events considered here. (Migration of turning arrivals using a modified Kirchhoff scheme has been commonplace for many years for imaging steep salt walls, but such vertical-velocity-gradient “V(z)” schemes will

not image double-bounce arrivals.) In the simplified velocity field used here for modeling, we have omitted the velocity inversion and reduced the overall compaction gradient in the overburden sediments. In the Balder and chalk layers, however, we do have strong vertical-compaction gradients, and they will produce turning arrivals. The production migration for the real data was conducted using 3D one-way wave-equation anisotropic migration, and a research study also was performed using transverse isotropy with a vertical axis (VTI) anisotropic 3D RTM code. For simplicity, here we are using 2D isotropic modeling and 2D isotropic RTM.

For the geometry considered here, the events of primary interest include (1) a single bounce at the flat-lying parts of the top Balder and top chalk reflectors, (2) a single bounce at the dipping parts of the top Balder and top chalk reflectors, (3) a noncrossing double bounce involving the flat and dipping parts of each of these reflectors, (4) a crossing double bounce involving the flat and dipping parts of each of these reflectors, and (5) events passing into the salt, including a bounce within the salt and a subset of these that later reflects from the flat reflector on its return path.

The last class of events is of less interest here because the transmission and reflection coefficients encountered by through-salt ray-paths gives rise to very low-amplitude events compared with events

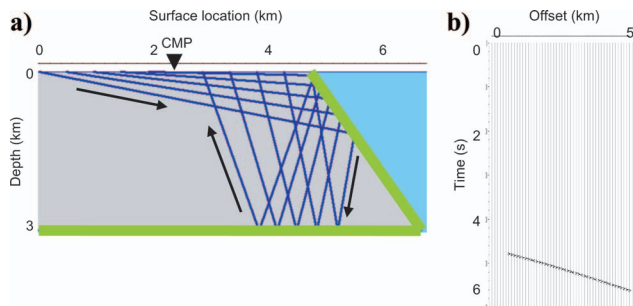


Figure 3. (a) Acute-angle, crossing events. Model horizons in green. (b) The associated CMP gather. Arrivals are present on most offsets, with arrival time increasing with offset.

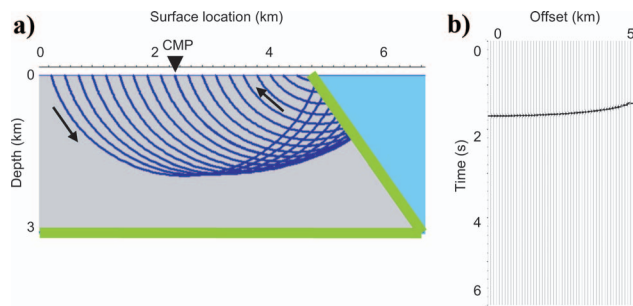


Figure 4. (a) Acute-angle reflector with a vertical compaction velocity gradient; turning events. Model horizons in green. (b) The associated CMP gather. Arrivals show that arrival time is decreasing with offset.

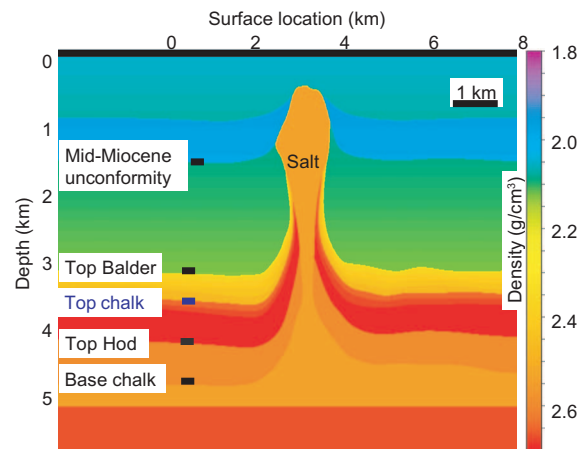


Figure 5. Density profile from the crestal line characterizing the North Sea salt diapir.

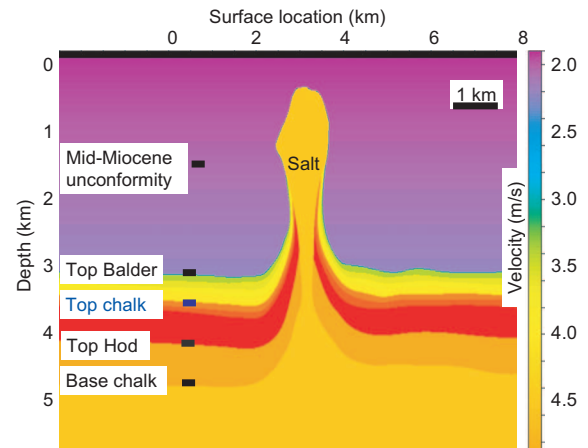


Figure 6. Interval-velocity profile from the crestal line characterizing the North Sea salt diapir.

involving reflections from the salt and other high-velocity-contrast events. In Figure 7 we show some of these raypaths and CMP gathers, from the left of the dome, that exemplify the moveout behavior for this geometry. The left side of Figure 7b shows the ray-traced events as indicated by the raypaths on Figure 7a, whereas the right side of Figure 7b shows the corresponding gathers produced by full elastic FD modeling. The events that have traveled in the salt are present but possess insignificant amplitude compared with other classes of arrival.

It is well-known from the Knott-Zoeppritz equations (Pelissier et al., 2007) that we will get large reflection amplitudes for some high grazing angles at large-velocity-contrast interfaces. In the case of double bounces, we can record arrivals with higher angles than we can for single-bounce events for a given surface offset, so we can have some unusual arrival strengths in the data. Also, for a medium with a shear velocity that is greater than the compressional wave velocity in the layer above it (such as may occur at a sediment-salt interface), we have two critical angles at their interface: the usual one for  $\Theta_{crit,P} = \sin^{-1}(V_{inc,P}/V_{refr,P})$ , and a second one for  $\Theta_{crit,S} = \sin^{-1}(V_{inc,P}/V_{refr,S})$  (see, for example, Muller, 2007, p. 71). In this instance we have a strong increase in the transmitted converted mode ( $T_{PS}$ ), which can give rise to important base-salt events propa-

gating as S within the salt. Sometimes these can be used for interpretation after migration with the shear velocity in the salt (Lewis, 2006). However, in this study we are considering only the P arrivals, although analyses of these converted events in another study were the main reason for using elastic FD modeling here (otherwise, we believe that acoustic modeling would have been adequate for the purposes of this paper).

We can gain insight into the relative amplitude behavior of these events by solving the Knott-Zoeppritz equations (here, we use an applet courtesy of the CREWES consortium). In Figure 8, we show the amplitude versus incidence angle for a P-wave incident on a sediment-salt interface (a) and on a salt-sediment interface (b), for the transmitted and reflected events. For low-velocity sediment in which sediment velocity is lower than the shear-wave velocity in the salt, we observe two critical angles (one for each of the transmitted P- and S-waves).

In Figure 9 we consider the more important raypaths, and we show an associated CMP gather in Figure 10. From the ray-tracing exer-

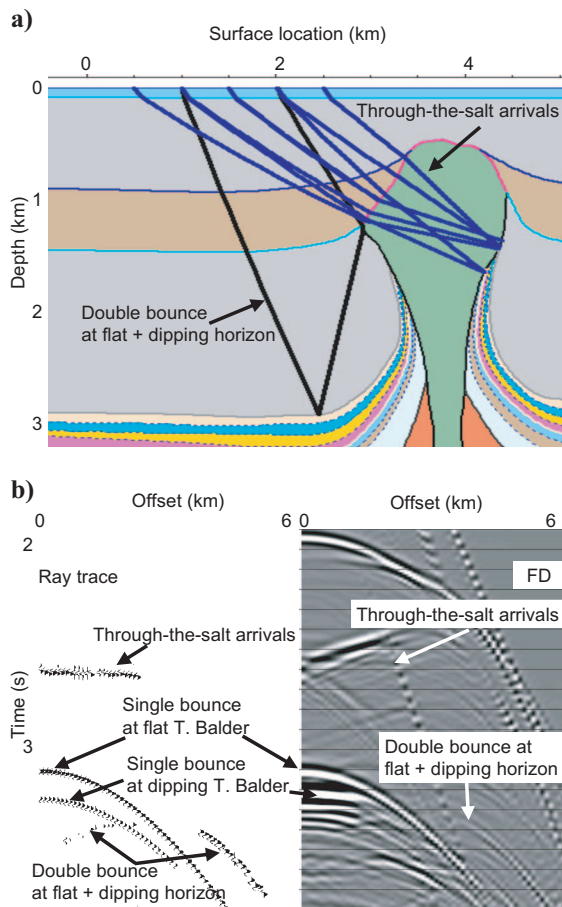


Figure 7. (a) Raypaths through the salt, illuminating the steep salt flank from within (in blue) and double-bounce events (in black). Other arrivals are omitted to avoid clutter but are included in the CMP gathers. (b) Ray-traced events and elastic FD (for CMP 1240, at surface location 1.5 km). The through-salt arrivals are comparatively weak.

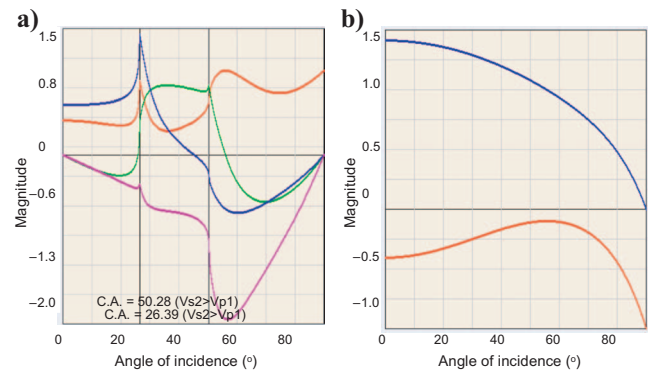


Figure 8. Amplitude versus incidence angle for an incident P-wave. (a) The sediment-to-salt response. (b) The salt-to-sediment response. Blue is the transmitted P, red is the reflected P, green is the reflected S, and purple is the transmitted S. For the sediment,  $V_p = 2000$  m/s,  $V_s = 1100$  m/s, and  $\rho = 2.05$  g/cm<sup>3</sup>. For the salt,  $V_p = 4500$  m/s,  $V_s = 2600$  m/s, and  $\rho = 2.17$  g/cm<sup>3</sup>.

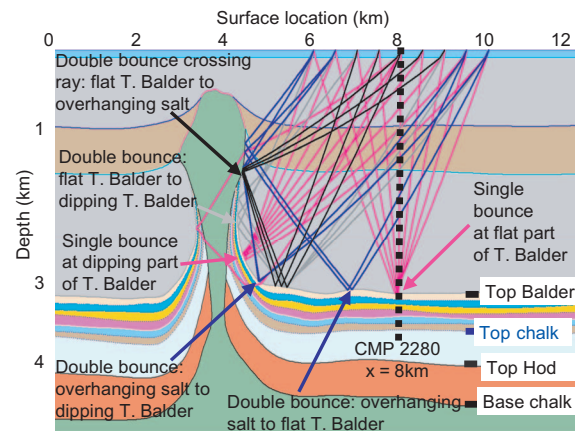


Figure 9. Plot of a few sparse rays shown against the interval-velocity model. The sediment velocity (in gray) ranges from approximately 1900 m/s to 2200 m/s, with some shallow impedance-contrast events. The absence of a strong sediment gradient precludes turning rays in the sediments, although a strong compaction velocity gradient below the top Balder and top chalk does produce turning rays. The salt velocity (green) is 4500 m/s, the upper chalk velocity is about 5700 m/s, and the lower chalk velocity is about 4900 m/s.

cises we can see clearly which are the single-bounce events and which are the double-bounce events illuminating the salt flank. The weak events passing through the salt body itself and illuminating the salt flank are omitted from the diagram to avoid clutter. Figure 10 shows a single CMP gather (surface location 8 km, CMP number 2280), as indicated in Figure 9, for (a) the ray-traced data and (b) the FD data. From the ray tracing, we can identify the moveout trajectories corresponding to each raypath.

Figure 11 shows a CMP gather at a nearby location (2240), for (a) ray tracing (including the first free-surface multiples and double bounces) and (b) the elastic FD modeling (without free-surface multiples but including all internal multiples). These comparisons show clearly why it is necessary to perform ray-trace modeling for individual sets of events. Otherwise, it is too difficult to understand what we are seeing in the FD data.

To see where these different classes of events appear in a stacked section, we show the stack of the elastic FD data in Figure 12. Figure 13 is an enlargement of the diffraction tails on the right flank of the dome indicated by the box in Figure 12. The enlargement is for the FD data and also for the ray-trace data omitting double bounces and the ray-trace data including double bounces. As expected, the wavelet character of the double-bounce events is heavily distorted during stacking. That is the result of such events not stacking properly be-

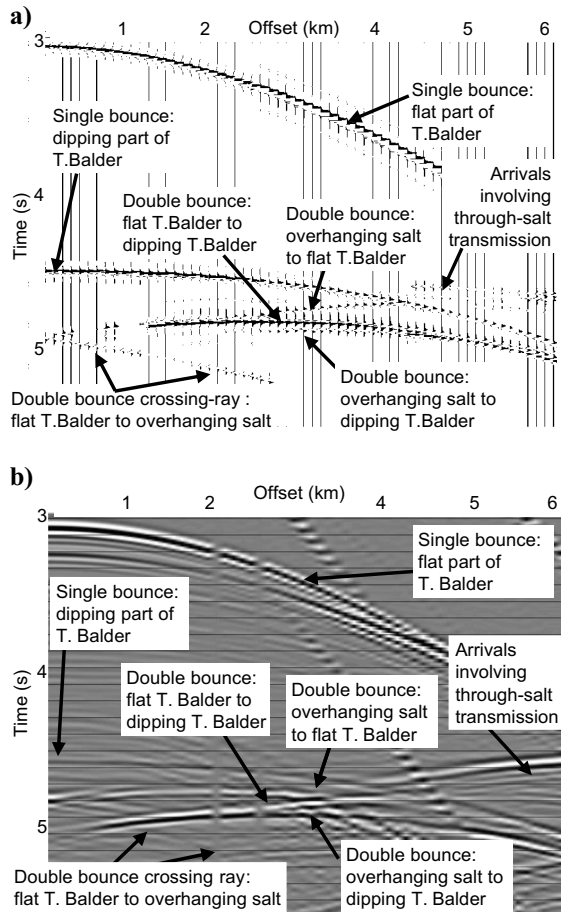


Figure 10. A single CMP gather (CMP number 2280, at surface location 8 km, as indicated in Figure 9) for (a) the ray-traced data and (b) the FD data. From the raypaths identified in Figure 9, we can identify the corresponding arrivals in the CMP.

cause of their anomalous moveout behavior. The stacks are produced by using the rms velocity associated with the interval-velocity model and not by using stacking-velocity analysis, and they have a mute of the direct-arrival energy.

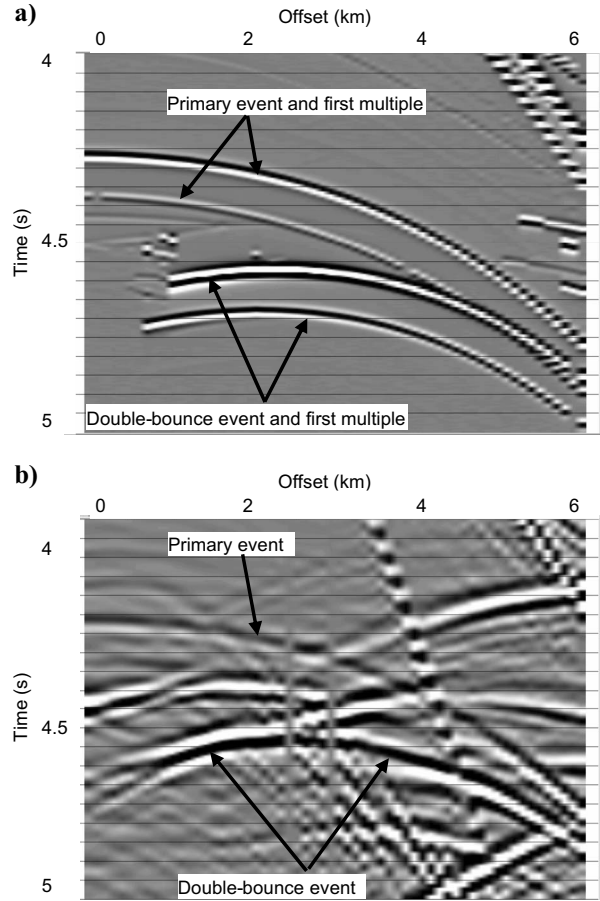


Figure 11. CMP gather number 2240, for (a) the ray-traced data with double bounces (also including the first free-surface multiple) and for (b) the FD data (without free-surface multiples).

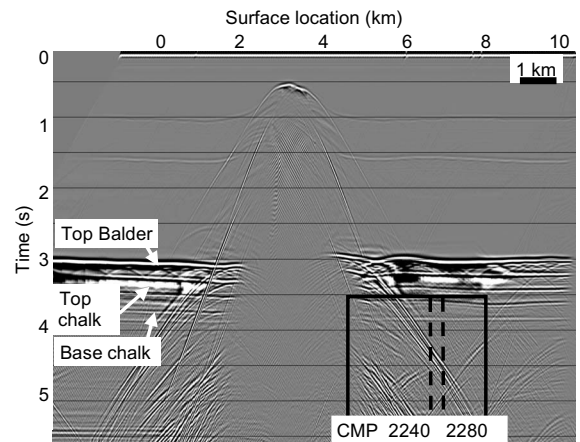


Figure 12. Stack of the elastic FD data. Box shows an area that is enlarged in Figure 13.

PREPROCESSING

Essentially, we are looking at processes that discriminate against events that exhibit anomalous moveout behavior in the CMP domain. For conventional 2D geometry, such events (in a one-way wave-propagation paradigm) constitute diffracted multiples and scattered energy. In other words, they are events that from a one-way perspective appear to have secondary source locations. Such events are classes of two-way wave propagation, in that the raypath undergoes a complete change of direction (such as an additional bounce or turning) before or after its main reflection from the interface of interest.

We began by assessing an apex-shifted multiple-attenuation routine (designed to attenuate events whose apexes are shifted from zero offset in CMP gathers: Trad, 2003; Stewart, 2004) as a first-order approximation to 3D surface-related multiple elimination (SRME) (Verschuur et al., 1992). By design, this effectively eradicates the double-bounce events.

The effects of these processing sequences are shown in the next figures for a set of CMP gathers straddling the salt dome. Figure 14 shows the raw-input FD-modeled data, and Figure 15 shows the output from the apex-shifted demultiple technique. Apex-shifted events are partially attenuated (better so on the left side of the salt dome).

We then assessed a  $\tau$ - $p$  mute (to attenuate backscattered noise). Normally, this is performed in conjunction with a deconvolution. Here we did not apply the deconvolution step, so we could isolate and highlight the effect of the  $\tau$ - $p$  mute. Also, because we used an absorbing-surface boundary condition in the FD modeling, we did not have direct short-period water-bottom multiples in the elastic FD data.

Figure 16 shows the output from  $\tau$ - $p$  muting. For the input to migration, a combination of both the apex-shifted and  $\tau$ - $p$ -muting processes was used. Apex-shifted events were attenuated successfully on both sides of the salt dome. This would be considered a good thing for conventional processing but is deleterious for two-way imaging.

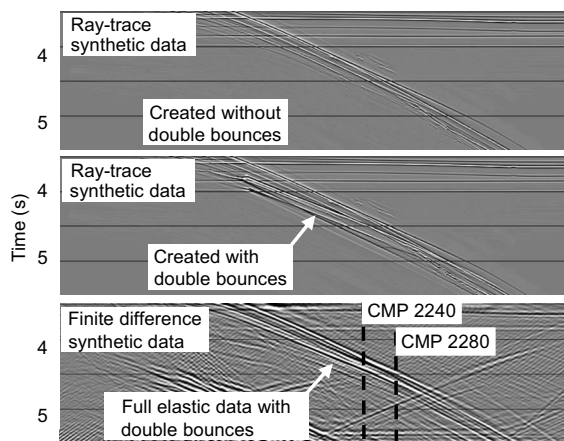


Figure 13. Detail of CMP stacked sections for the ray-traced synthetic data with and without double bounces, and for the FD data (from the box indicated in Figure 12), showing locations of double-bounce events in diffraction tails. Also noted are the locations of CMPs 2240 and 2280. For this study we did not perform any stacking velocity analysis, so the data have been stacked simply using the rms version of the interval-velocity model.

Lastly, we assessed a Radon demultiple. If we were to employ the Radon filter to output the multiple-free primaries directly, we would have a problem because all apex-shifted events would be compromised. However, this issue can be circumvented if we use the Radon

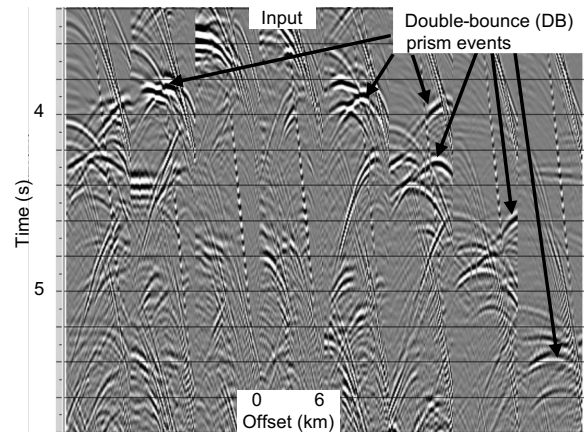


Figure 14. A selection of raw-input CMP gathers from the FD-modeled data straddling the dome.

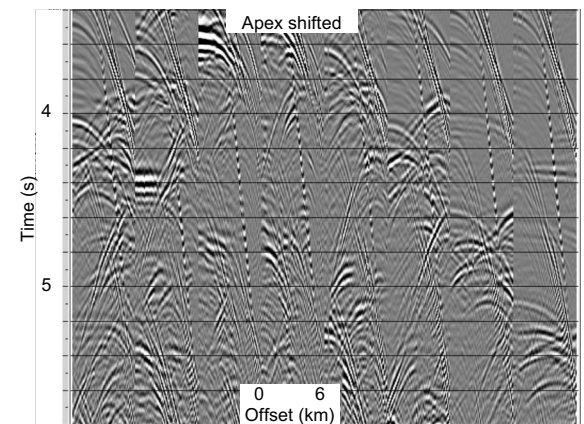


Figure 15. CMP gathers output from the apex-shifted demultiple technique, which performed well on the left of the dome.

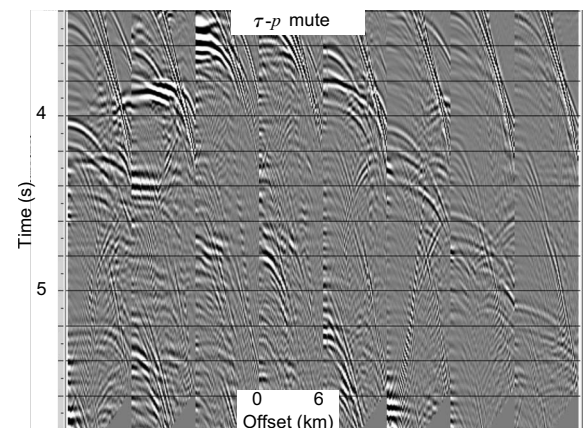


Figure 16. CMP gathers output from  $\tau$ - $p$  muting. This performed better on the right of the dome. Apex-shifted events are attenuated successfully. This would be considered a good thing for conventional processing. Data with a combination of apex-shifted demultiple and  $\tau$ - $p$  muting were input later to the RTM tests.

transform to model the multiples and then adaptively subtract these from the input data. Working in this way, we would preserve the apex-shifted arrivals in the CMP gather. Figure 17 shows a Radon output, preserving conventional “primaries only.” In industrial practice, we usually would not do this.

DISCUSSION

In Figure 18 we see the RTM of the FD raw data, using a slightly smoothed model with some postprocessing to enhance the image. In practice, we never could obtain such a perfect image because we always would have residual errors in the velocity model. In an industrial flow, in which we are trying to determine the model, we would approach the definition of the salt flank using a migration with a salt-free model. In this case, the RTM imaging condition will produce an image of the salt flank from double-bounce events as long as the flat-lying high-velocity-contrast layers are present in the model. The image of the steep events derived in this way would be weaker than if we had both the flat and the steep horizons defined in the model, because we would be imaging only with energy that had reflected first from the flat event and we would be missing the energy that reflected

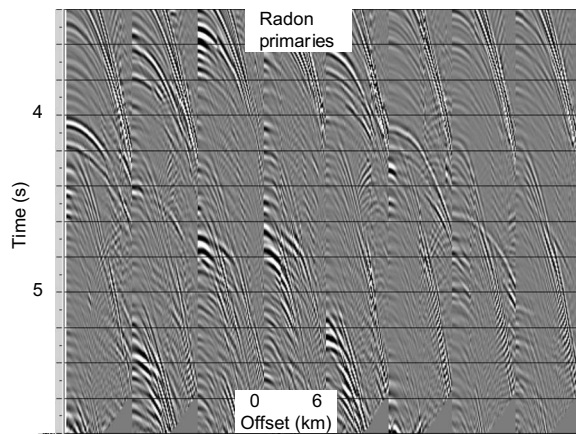


Figure 17. The Radon filter, preserving conventional primary events.

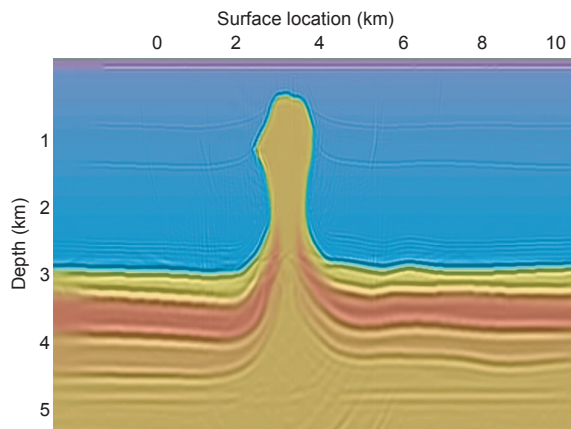


Figure 18. RTM with the raw data and salt interval-velocity model.

first from the steep horizon. Also, if we were in a geologic setting with strong vertical compaction velocity gradients, the RTM could image the salt-flank events using turning-wave energy. Thus, to evaluate the effect of our preprocessing on the imaging of the double-bounce arrivals, we compare results using RTM with a no-salt model.

Figure 19 shows the image of the raw data with the no-salt model. In both Figures 18 and 19, the interval-velocity model used in the migration is superimposed. Figure 20 repeats Figure 19 but without the color model overlay, and Figure 21 shows the RTM image using the no-salt model of the data subjected to a  $\tau$ - $p$  mute and apex-shifted demultiple. Clearly, the vertical and overturned salt-flank events have been seriously attenuated in the latter sequence.

The interaction of RTM with multiples is an interesting one: In principle, if we correctly model the propagation of all multiples, a correct two-way imaging algorithm should collapse the multiple wavefield back to the primary-reflection locations. However, as [Mittet \(2006\)](#) noted, approximations in our boundary conditions mean

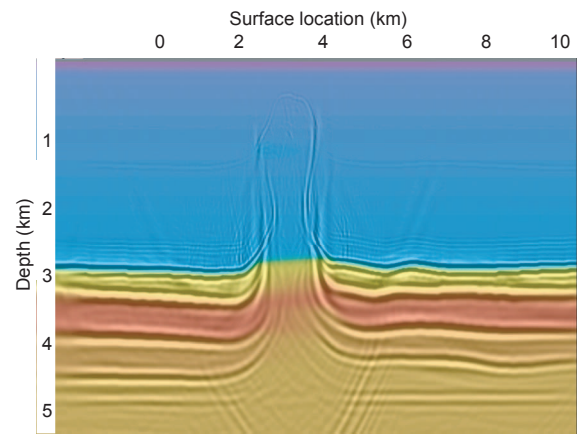


Figure 19. RTM with the raw data and the no-salt model. The salt-wall image is stronger in the no-salt model because we avoid the (correct) model-imposed wavelet stretch at the salt boundary. The imaging condition still constructs the salt-wall event because we have one bounce point specified in the model (the flat-lying top Balder).

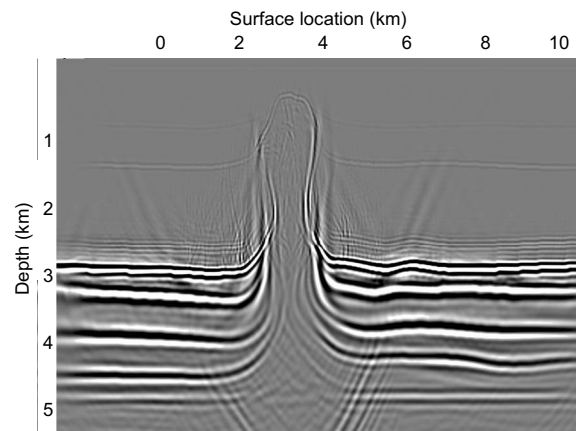


Figure 20. Same RTM image of the raw data as in Figure 19, but here without the superimposed color model. We have good imaging of the overturned salt flank (the wavelet looks better than with the correct model because the wavelet is not stretched by the salt interface).

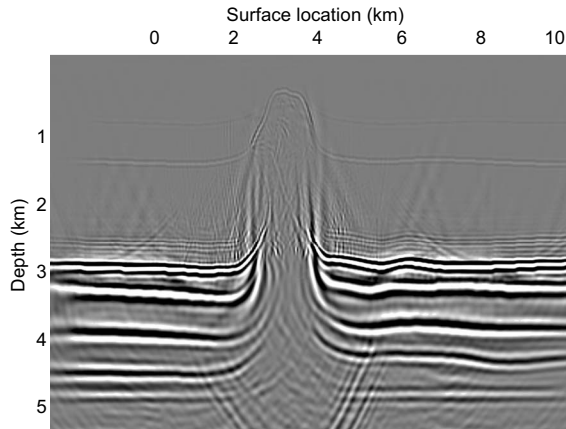


Figure 21. RTM image of the data processed with apex-shifted demultiple and  $\tau$ - $p$  muting. The overturned salt-wall reflectors have been damaged significantly by this conventional preprocessing flow.

that our amplitude treatment is not exact. Furthermore, given that we are still using only an acoustic approximation, the energy partition between P and S events at each interface will be incorrect, and we will not deal correctly with amplitudes. This is especially important for the multiples that undergo more than one interaction with an interface. Whereas adaptive subtraction procedures in multiple-suppression algorithms can attempt to address the issue of imprecise amplitude (and phase), a two-way acoustic imaging algorithm might have problems. We have seen some encouraging results for imaging multiples, but to date we still recommend employing multiple suppression (typically using 3D SRME) prior to imaging with RTM.

## CONCLUSIONS

Conventional preprocessing is designed to remove various classes of noise, such as backscattered energy, multiples, and diffracted multiples. The processes designed to do this have, for the most part, been designed with one-way wave propagation of primary energy in mind. Software developers have spent several years developing routines that efficiently remove diffracted multiples and backscattered noise, developing the apex-shifted approach, and more recently, developing 3D SRME.

However, if we set out to migrate two-way propagated primary energy, as is now possible with the new generation of migration algorithms (such as RTM), we need to ensure that our preprocessing flow is fit for purpose and does not inadvertently damage the very events we are trying to image. Typically, two-way propagated primary events (such as double bounces) appear in the CMP domain with their moveout apex shifted from zero offset. As such, they resemble diffracted multiples or backscattered energy. Consequently, to avoid unnecessary removal of useful primary (two-way) energy, tools such as 3D SRME must be employed instead of more conventional 2D approaches when one is dealing with multiple suppression in complex environments.

## ACKNOWLEDGMENTS

I wish to thank my colleagues at ION GX Technology for useful discussions, and especially Mike Goodwin, Stuart Greenwood, and Brent Mecham for help with creating the synthetic data, and Dave King, Mick Sugrue, and Ivan Berranger for discussions and help

with the RTM jobs. My thanks go also to the SEG reviewers Yonghe Sun, Samuel Gray, and John Etgen, and Associate Editor Isabelle Lecomte, for their helpful suggestions that significantly improved this paper. Thanks also to the management of ION GX Technology for permission to publish the results of this study.

## REFERENCES

- Baysal, E., D. D. Kosloff, and J. W. C. Sherwood, 1983, Reverse-time migration: *Geophysics*, **48**, 1514–1524.
- Bednar, J. B., K. Yoon, C. Shin, and L. R. Lines, 2003, One-way vs two-way wave equation imaging—Is two-way worth it?: 65th EAGE Conference and Exhibition, Extended Abstracts, B11.
- Bernitsas, N., J. Sun, and C. Sicking, 1997, Prism waves—An explanation for curved seismic horizons below the edge of salt bodies: 59th EAGE Conference and Exhibition.
- Cavalca, M., and P. Lailly, 2005, Prismatic reflections for the delineation of salt bodies: 75th Annual International Meeting, SEG, Expanded Abstracts, 2550–2553.
- Davison, I., G. I. Alsop, N. G. Evans, and M. Safaricz, 2000, Overburden deformation patterns and mechanisms of salt diapir penetration in the Central Graben, North Sea: *Marine and Petroleum Geology*, **17**, 601–618.
- Farmer, P., I. F. Jones, H. Zhou, R. Bloor, and M. C. Goodwin, 2006, Application of reverse-time migration to complex imaging problems: *First Break*, **24**, No. 9, 65–73.
- Hale, D., N. R. Hill, and J. Stefani, 1992, Imaging salt with turning seismic waves: *Geophysics*, **57**, 1453–1462.
- Hawkins, K., C.-C. Cheng, S. A. Sadek, and M. A. Brzostowski, 1995, A  $v(z)$  DMO developed with the North Sea Central Graben in mind: 65th Annual International Meeting, SEG, Expanded Abstracts, 1429–1432.
- Jones, I. F., 2008, The effects of preprocessing on reverse-time migration—a North Sea study: *First Break*, **26**, No. 7, 73–82.
- Jones, I. F., M. Sugrue, D. King, M. Goodwin, I. Berranger, H. Zhou, and P. Farmer, 2006, Application of reverse-time migration to complex North Sea imaging: PETEX biennial meeting.
- Larsen, S. C., and J. C. Grieger, 1998, Elastic modeling initiative, part III: 3-D computational modeling: 68th Annual International Meeting, SEG, Expanded Abstracts, 1803–1806.
- Levander, A. R., 1988, Fourth-order finite-difference P-SV seismograms: *Geophysics*, **53**, 1425–1436.
- Lewis, J., 2006, The potential of mode-converted waves in salt interpretation: Presented at SEG/EAGE summer research workshop.
- Madariaga, R., 1976, Dynamics of an expanding circular fault: *Bulletin of the Seismological Society of America*, **66**, 639–666.
- McMechan, G. A., 1983, Migration by extrapolation of time-dependent boundary values: *Geophysical Prospecting*, **31**, 413–420.
- Mittet, R., 2006, The behaviour of multiples in reverse-time migration: 68th EAGE Conference and Exhibition, Presented at Workshop No. 6, Removing or Using Multiples?
- Muller, G., 2007, Theory of elastic waves: ebook, <http://www.gfz-potsdam.de/bib/pub/str0703/0703.pdf>, accessed September 2007.
- Pelissier, M. A., H. Hoerber, N. van de Coevering, and I. F. Jones, 2007, Classics of elastic wave theory: SEG Geophysics Reprint Series, No. 24.
- Shan, G., and B. Biondi, 2004, Imaging overturned waves by plane wave migration in tilted co-ordinates: 74th Annual International Meeting, SEG, Expanded Abstracts, 969–972.
- Stewart, P., 2004, Multiple attenuation techniques suitable for varying water depths: CSEG National Convention, abstracts: <http://www.cseg.ca/conventions/abstracts/2004/2004-abstracts-toc.cfm>, accessed August 19, 2008.
- Thomson, K., 2004, Overburden deformation associated with halokinesis in the Southern North Sea: implications for the origin of the Silverpit Crater: *Visual Geosciences*, **9**, 1–9.
- Trad, D. O., 2003, Interpolation and multiple attenuation with migration operators: *Geophysics*, **68**, No. 6, 2043–2054.
- Verschuur, D. J., A. J. Berkhou, and C. P. A. Wapenaar, 1992, Adaptive surface related multiple elimination: *Geophysics*, **57**, 1166–1177.
- Virieux, J., 1986, P-SV wave propagation in heterogeneous media—Velocity-stress finite-difference method: *Geophysics*, **51**, 889–901.
- Whitmore, N. D., 1983, Iterative depth migration by backward time propagation: 53rd Annual International Meeting, SEG, Expanded Abstracts, Session S10.1.
- Yoon, K., C. Shin, S. Suh, L. R. Lines, and S. Hong, 2003, 3D reverse-time migration using the acoustic wave equation: An experience with the SEG/EAGE data set: *The Leading Edge*, **22**, No. 1, 38–41.
- Zhou, H., G. Zhang, and R. Bloor, 2006, Anisotropic acoustic wave equation for VTI media: 68th EAGE Conference and Exhibition.
- Zhang, Y., X. Sheng, and G. Zhang, 2006, Imaging complex salt bodies with turning-wave one-way wave equation: Presented at SEG/EAGE summer research workshop.